Calibrating and evaluating a range camera for Cultural Heritage metric survey

International Journal of Hydrogen Energy 227 (2026) 154634

Contents lists available at ScienceDirect

International Journal of Hydrogen Energy

journal homepage: www.elsevier.com/locate/he

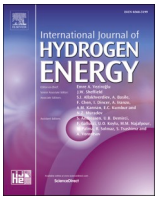

CFD-supported calibration optimization of a retrofit hydrogen–diesel dual-fuel engine

B. Peiretti Paradisi [a,*], A. Piano [a], F. Millo [a], F. Accurso [b], F.C. Pesce [b], A. Vassallo [b]

[a] Energy Department, Politecnico di Torino, Italy
[b] Dumarey Automotive Italia, Italy

A B S T R A C T

Dual-fuel (DF) hydrogen–diesel engines could offer a retrofit-compatible pathway for medium-/heavy-duty transport decarbonization. In this study, a 6-cylinder compression ignition engine retrofitted for hydrogen port fuel injection is investigated through a CFD-supported framework. A validated 3D-CFD model, based on an extensive experimental dataset, was applied to investigate injection strategies and calibration parameters in both retrofit and native DF engine modes. The model accurately captures combustion behavior, emissions trends, and the factors limiting hydrogen energy share (HES). Results show that an optimized native DF calibration enables up to 90% CO_2 reduction relative to diesel operation while maintaining combustion stability. Particulate matter emissions are nearly eliminated at high HES, whereas low HES combined with non-optimized diesel injection results in PM levels comparable to diesel-only operation. The analysis highlights the decisive role of a coordinated optimization of HES and diesel calibration strategy in governing ignition dynamics, combustion efficiency, and soot formation.

1. Introduction

In the current context of decarbonization, driven by stringent emission regulations already in force (EURO VI) and the forthcoming EURO VII standards, the transport sector is called to adopt solutions that reconcile performance and environmental sustainability [1]. Despite the rapid advancement of electrification, significant technical, economic, and infrastructural barriers still limit the large-scale adoption of battery-electric powertrains in several specific applications [2]. Various studies have identified high upfront capital costs, excessive battery weight (which reduces payload), limited charging infrastructure, and grid constraints as the main barriers to electrification in the medium- and heavy-duty sectors [3]. Consequently, alternative fuels represent a concrete pathway toward reducing pollutant emissions and achieving substantial CO_2 mitigation, in line with the European Union's Fit for 55 package, which targets a 55% reduction in net greenhouse gas emissions by 2030 and carbon neutrality by 2050 [4].

Among the available energy vectors, the employment of renewable hydrogen has emerged as one of the most promising alternatives to conventional fossil fuel for a decarbonized transport sector [5]. Its carbon-free molecular structure allows for near-zero tailpipe CO_2 emissions, while its wide flammability limits (4–76 vol%), high Lower Heating Value (LHV) and high diffusivity enable the conditions for a fast and stable combustion with high thermal efficiency [6]. In addition, hydrogen Internal Combustion Engines (ICEs) can leverage the extensive existing ICE infrastructure, offering fast refueling times, high durability, and reduced implementation costs compared with fuel cell or battery electric solutions [7,8]. These features make hydrogen particularly suitable for medium- and heavy-duty transport sectors, where the need for operational flexibility and long driving range remains crucial.

However, the use of hydrogen in ICEs also introduces several challenges. The high laminar flame speed, low ignition energy, and elevated flame temperature of hydrogen can lead to increased NO_x emissions and abnormal combustion phenomena such as pre-ignition or knocking, especially under stoichiometric conditions [9]. Operating with ultra-lean mixtures has proven effective in mitigating these issues by lowering in-cylinder temperatures and enhancing knock resistance [10]. Nevertheless, the very high auto-ignition temperature of hydrogen (≈858 K) prevents its direct use in Compression Ignition (CI) engines [11]. For this reason, Dual-Fuel (DF) operation, where a small amount of diesel acts as a pilot to ignite hydrogen combustion, emerges as a practical and efficient strategy, combining the benefits of CI operation with the clean potential of hydrogen [12].

In a DF hydrogen–diesel configuration, hydrogen is typically introduced in the intake ports via Port Fuel Injection (PFI), forming a premixed charge with air, while a small amount of diesel is directly injected into the cylinder near top dead center. The diesel acts as a pilot fuel, starting the combustion by auto-ignition and triggering the flame propagation of the hydrogen–air mixture [13]. This strategy combines the efficiency advantages of CI engines with the environmental benefits

* Corresponding author.
E-mail address: benedetta.peiretti@polito.it (B. Peiretti Paradisi).

https://doi.org/10.1016/j.ijhydene.2026.154634
Received 9 January 2026; Received in revised form 16 March 2026; Accepted 18 March 2026
Available online 21 March 2026

of hydrogen substitution, offering a flexible and cost-effective route to reduce CO_2, CO, HC, and PM emissions while preserving engine architecture and reliability [14]. A further advantage is the potential for retrofitting existing diesel engines, as only minor modifications to the injection system and fuel supply hardware are required. This makes the DF concept particularly attractive from an industrial and economic perspective, allowing the reuse of well-established engine platforms and facilitating a faster deployment of hydrogen-powered solutions in the current vehicle fleet.

Different research studies on hydrogen-diesel DF combustion systems are present in literature, focused on experimental characterization in single-cylinder research engines, together with numerical modeling and practical implementation in real-world applications. In particular, calibration parameters influencing both the DF combustion behaviour and the emissions formation have been assessed in the last years, and here the main results are summarized.

Vavra et al. [15], investigated the potential of hydrogen as the primary fuel in a DF CI engine equipped with a hydrogen PFI, operating across a wide range of engine speeds and loads. Results demonstrated that increasing the Hydrogen Energy Share (HES) up to 98% led to substantial reductions in CO_2, CO, and Particulate Matter (PM) emissions, proportional to the decrease in carbon content of the fuel. The reduction in PM formation was attributed to hydrogen's carbon-free nature and the more homogeneous, high-temperature combustion process, which limits soot formation in fuel-rich zones and promotes soot oxidation. Only at very high loads, where hydrogen displaced part of the intake oxygen, was a slight PM increase observed. NO_x emissions remained comparable to those of conventional diesel operation, while indicated efficiency showed a modest reduction at the highest substitution levels, mainly due to incomplete combustion at low loads.

Tsujimura et al. [16] experimentally tested a single-cylinder retrofitted hydrogen–diesel DF engine equipped with hydrogen PFI, varying load, speed, and HES. Increasing HES enhanced indicated thermal efficiency at medium to high loads, achieving over 40% efficiency when hydrogen accounted for more than 50% of input energy. However, at low loads, incomplete combustion and high unburned hydrogen emissions were observed due to overly lean mixtures. Despite significant reductions in CO_2 and soot, NO_x emissions slightly increased with HES because of higher local combustion temperatures, although EGR effectively mitigated this effect.

Following experimental findings, several studies have numerically examined the impact of hydrogen substitution and injection strategy on performance and emissions. Tripathi et al. [17] employed 3D-CFD simulations to optimize diesel injection strategies in a hydrogen DF CI engine, validating their model against experimental data for a 19.5:1 compression-ratio single-cylinder engine. The analysis demonstrated that a split-injection strategy with optimized pilot mass could achieve a favorable trade-off between efficiency and emissions. Advanced injection timings improved combustion completeness and reduced CO and HC emissions, while excessive advancement increased pressure rise rates and NO_x formation due to higher temperatures. Soot emissions decreased significantly with earlier injection timing and with higher HES, as hydrogen's absence of carbon and high diffusivity suppressed rich fuel pockets responsible for soot precursors. Split injections further reduced soot through improved air–fuel mixing and more uniform combustion.

Similarly, Scrignoli et al. [18] numerically investigated hydrogen–diesel DF operation in a light-duty CI engine using 3D-CFD simulations validated against experiments. Their study analyzed diesel replacement up to 80% at partial and full loads, revealing that moderate HES (≈40%) improved brake thermal efficiency and indicated mean effective pressure due to faster combustion and enhanced mixture homogeneity. However, at higher substitution levels, incomplete combustion and steep pressure gradients limited performance and stability. Optimization of diesel Start Of Injection (SOI) proved essential for maintaining efficiency and combustion stability, as advanced SOI improved performance at low HES, whereas retarded SOI mitigated excessive pressure rise and knocking at high HES.

Maroteaux et al. [19] combined experimental and simulation analyses on a single-cylinder optical engine operating at 1500 and 2000 rpm varying also the EGR rate. Results showed that increasing the diesel mass in the pilot injection extended combustion duration and increased NO_x formation, while the use of EGR reduced NO_x emissions by about 50%. The mass split between pilot and main injections had negligible influence on ignition delay, confirming that hydrogen dominates the early flame propagation phase. PM and carbon-based emissions became negligible due to hydrogen's carbon-free structure and its high diffusivity, which enhance mixture homogeneity and prevent soot formation.

Focused on medium- and heavy-duty applications, Guan et al. [20] demonstrated through an extensive experimental campaign the feasibility of retrofitting a hydrogen–diesel DF system on a commercial Class-8 heavy-duty truck without altering the original diesel injection system or Engine Control Unit (ECU). HES up to 30% were achieved with proportional CO_2 reductions and negligible impact on brake-specific energy consumption. However, results revealed that air-path management and injection control strategies are crucial to prevent increased CO and PM emissions at high load due to local oxygen depletion.

Lee et al. [21] using high-speed optical diagnostics, characterized a diesel-piloted hydrogen DF concept in a heavy-duty engine, observing that hydrogen presence in the premixed charge inhibits pilot ignition and increases cycle-to-cycle variability. Complementary simulations indicated that maintaining locally rich pilot regions supports stable ignition, highlighting the critical coupling between mixing and ignition chemistry.

Collectively, these studies demonstrate that the hydrogen–diesel DF concept can be effectively adapted across a wide range of ICE applications, from light commercial to heavy-duty transport, also through retrofit solutions. Despite the present experimental and numerical research on hydrogen–diesel DF combustion, key uncertainties remain regarding the complex interaction between the diesel fuel injection strategy and the premixed hydrogen–air charge, and their combined impact on ignition behaviour, combustion efficiency, and pollutant formation. In particular, the decisive role of diesel calibration parameters, including injection timing, pressure, and mass, in governing ignition dynamics and soot abatement has not yet been systematically investigated all together. Moreover, most existing models have been validated only on single-cylinder setups or simplified geometries, limiting their predictive capability for full-scale engine architectures. Additionally, the synergistic optimization of HES and dedicated diesel injection strategies, as well as the comparative influence of injection timing, EGR rate, and calibration approach between retrofit and native DF configurations, has not been explored for the same case study. Addressing these gaps requires accurate, experimentally validated CFD frameworks capable of capturing the coupled chemical–fluid dynamic phenomena that govern ignition delay, heat release rate, and pollutant formation across different HES and calibration strategies. In this context, in the present study a 3D-CFD numerical platform has been developed and calibrated against an extensive experimental dataset, with the aim of investigating the combustion and emission behavior of a hydrogen–diesel DF engine under two representative configurations.

(i) a **retrofit DF mode**, in which hydrogen is added to an existing diesel engine with minimal modifications, without modifying the diesel injection strategies, in order to ensure a flexible switch to Diesel Only (DO) mode of the engine.
(ii) a **native DF calibration**, specifically optimized for hydrogen operation, employing DO as a pilot fuel to premix and ignite the hydrogen combustion.

The analysis aims to provide a comprehensive understanding of the combustion process, and emission characteristics associated with both approaches, thereby outlining the potential and practical limitations of

hydrogen dual-fuel technology in different calibration procedures, as a viable near-term pathway toward a new generation of DF hydrogen-diesel combustion systems.

The remainder of this paper is organized as follows. Section 2 describes the experimental setup and dataset used for the calibration of the simulation framework. Section 3 details the 3D-CFD modeling approach, including mesh setup, submodels, and chemical kinetics. Section 4 presents the validation of the numerical model against experimental data and discusses the main results on combustion behavior, efficiency, and emissions for both retrofit and native DF configurations. Finally, Section 5 summarizes the main conclusions and outlines future research directions for optimizing hydrogen–diesel dual-fuel systems.

2. Case study and available experimental data

The engine selected for the analysis is an inline six-cylinder CI engine equipped with a variable geometry turbocharger, developed for medium-heavy duty applications by Dumarey Automotive Italia [22]. The engine has been retrofitted to a DF configuration from a state-of-the-art diesel engine and modified to allow for H2 injection, with a PFI system installed on the intake manifold. The fuel rail, sensors and injectors were also installed on the intake manifold, leveraging the flexibility of the additive manufacturing process. The original diesel combustion system was not modified, thus the maximum performance is maintained when the engine is operated in diesel mode. The main engine specifications are reported in Table 1.

The experimental campaign was carried out at Dumarey Automotive Italia and taken as a basis for the calibration and validation of the 3D-CFD simulation platform. The test matrix was designed to investigate a wide range of HES. In particular, the HES is defined as in Eq. (1):

$$HES = 100\,\frac{\dot{m}_{H_2}\,LHV_{H_2}}{\dot{m}_{H_2}\,LHV_{H_2} + \dot{m}_{diesel}\,LHV_{diesel}}, \qquad \text{Equation 1}$$

where the LHV is the lower heating value of the fuel and $\dot{m}$ the fuel mass flow rate.

In the initial phase of the experimental investigation, a pure retrofit approach was adopted: besides installing the PFI injectors, the only modification consisted of reducing the diesel injection pressure to partially substitute diesel with hydrogen, while maintaining constant injection duration. The injection strategy defined by the ECU was preserved, enabling HES of up to 55% in the engine map without inducing combustion instability. In the second phase, a more flexible ECU calibration was implemented, obtaining a native DF calibration by reducing diesel injection to a single pilot event, allowing for higher HES. In this configuration, a conventional DF combustion mode was achieved, characterized by port fuel injection of gaseous hydrogen with a subsequent premixed combustion ignited by a small amount of diesel. Accordingly, two distinct Operating Modes (OMs) of the engine are defined: OM1, corresponding to the pure retrofit configuration, and OM2, representing the native DF operation. To validate the simulation setup and analyze the DF combustion behavior, one engine Working Point (WP) was selected at low load (WP: 2500 rpm × 6 bar BMEP). The WP was chosen to represent a wide range of HES and to ensure the availability of extensive experimental data from calibration parameter sweeps (i.e., EGR rate, diesel SOI), as can be seen in Table 2. The calibration parameters in terms of SOI and EGR rate are expressed as a variation with respect to the baseline DO. The DO operates at medium EGR rate level.

Table 1
Engine technical specifications.

Displacement	3.0 L
Cylinders	6
Bore x Stroke	84 mm × 90 mm
Compression Ratio	15.2
Diesel inj. system	DI Common rail Pinj,max = 2000 bar
H2 inj. system	PFI Pinj,max = 8 bar

Table 2
Engine WP taken as a reference for the 3D-CFD model validation.

Speed [rpm]	BMEP [bar]	OM	HES [%]	ΔSOI main diesel [deg]	ΔEGR rate [%]
2500	6	DO	0	-	-
		OM1	30	0	−5
		OM2	90	−12; −9; −6;	−20; 0

Fig. 1 illustrates the injection strategies and fuel shares for the different OMs for the chosen engine condition (WP: 2500 rpm × 6 bar BMEP). The upper section of Fig. 1 shows the adopted injection rate, comparing DO operation (solid lines) with the native DF mode (OM 2, dashed lines) and the retrofit DF configuration (OM1, dotted lines). The lower section presents the corresponding energy contribution from the different fuels. Going from DO operation to the retrofit DF mode (OM1) reduces rail pressure and, consequently, diesel quantity while preserving the original injection pattern of two pilots, one main, and one post-injection. The reduced diesel contribution is compensated by PFI hydrogen, achieving approximately 30% HES at same load. In contrast, for native DF operation (OM2), diesel is injected only in a single pilot event, with HES up to 90%.

Combustion parameters obtained from the experimental campaign are shown in Fig. 2 for the previously analyzed engine WP (see Table 2) and three different HES: DO (HES = 0%), OM1 at 30% and OM2 at 90%. Specifically, from the top, the Ignition Delay (ID), the SOC, the crank angle corresponding to 50% of the Mass Fraction Burned (MFB50) and the combustion duration (MFB 10-90) are shown. For the OM2, all the parameters are mapped as a function of the main diesel SOI and EGR rate, while the results for the OM1 and DO operation are highlighted with a textbox in correspondence of the SOI of the main diesel injection. The ID is calculated as the difference between the SOC and the hydraulic

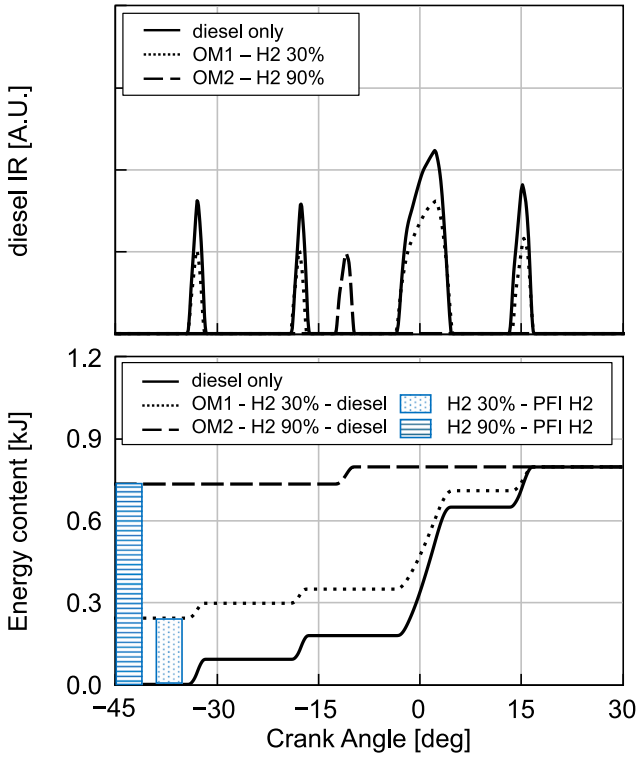

Fig. 1. Diesel injection rate (top) and energy content (bottom) for different HES and engine OMs. WP: 2500 rpm × 6 bar BMEP.

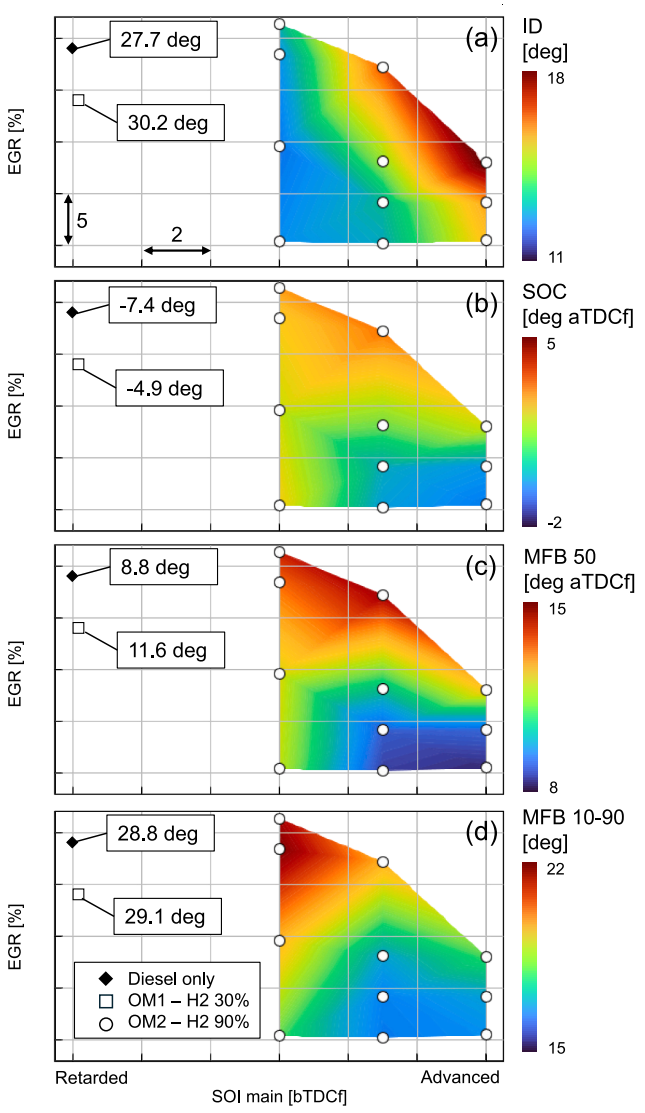

Fig. 2. Impact on combustion parameters of different HES and sweep of calibration parameters. (a) ID, (b) SOC, (c) MFB 50, (d) MFB 10-90.

SOI of the first diesel injection event.

Starting from the first combustion phases, OM1 exhibits a slightly longer ID with respect to DO operation, despite of the lower EGR rate, highlighting an inhibiting effect of hydrogen on the autoignition characteristics of the blend and a detrimental effect on the ID of the lower diesel injection pressure for the OM1. The situation is reflected also on the SOC values, with a retarded combustion for the OM1 with respect to DO conditions. However, both the mentioned OMs ignite prior to the main diesel injection event. The, for all the mapped conditions in OM2, the ID is always much larger than the diesel injection duration (almost 3 deg), ensuring a pure premixed combustion mode. Regarding the trend with the main calibration parameters for the OM2, the higher the EGR rate, while keeping the SOI constant, the higher the value of ID. Regarding the trend of ID with respect to SOI at constant EGR rate, the more advanced SOI the longer the ID, with a more pronounced ID increase at medium/high EGR rates. As a result, in terms of SOC the trend is the following: at medium/high EGR rate the impact of SOI variation on the SOC is almost negligible, counterbalancing the SOI advance with a longer ID and obtaining a SOC close to the TDCf for all the conditions. On the contrary, at low EGR rate advancing the SOI clearly advance the SOC, despite of the longer ID. It could be explained by a combination between the mixing time available for the evaporated diesel fuel and the in-cylinder thermodynamic conditions found during the diesel injection event, as already found in [23] for a DF marine engine. In particular, advancing diesel injection allows a favorable timing between the mixing process of diesel evaporated fuel and hydrogen/air with the pressure and temperature conditions in the cylinder, crucial to obtain a distribution of diesel fuel at reactive equivalence ratios close to the TDCf and ignite the blend. Moving to the MFB50, its behavior reflects the trend of the SOC for the OM2, with a more advanced center of combustion for low EGR rate and advanced SOI, and a postponed MFB50 for higher EGR rate and retarded SOI. Going ahead, at low/medium EGR levels, a minimum combustion duration is observed for a medium level of SOI; whereas at high EGR levels, advancing the SOI results in shorter combustion durations. For OM1, combustion is longer than that of OM2 and comparable to DO, highlighting a slower combustion process.

Then, in Fig. 3 the delta Coefficient of Variation (COV) of the IMEP with respect to DO operation are mapped as in Fig. 2 and for the same operating conditions. At first, higher COVs are evident in presence of hydrogen in the mixture with respect to DO mode varying all the calibration parameters, as already pointed out in [21]. In particular, the OM1 shows the maximum increase of COV with respect to DO, while a clear trend is present for the OM2 as a function of SOI. Finally, at medium/low EGR rate, the COV is comparable to the one of the DO mode.

Going ahead, in Fig. 4 the variation of equivalent Brake Specific Fuel Consumption ($BSFC_{eq}$) and CO_2 emissions with respect to DO operation are mapped as in Fig. 2 and for the same operating conditions. In particular, the $BSFC_{eq}$ is defined as in Eq. (2):

$$BSFC_{eq} = \frac{\dot{m}_{diesel}}{P_b(100 - \%HES)} \qquad \text{Equation 2}$$

where P_b is the engine brake power.

Across all working conditions, an increase in $BSFC_{eq}$ can be observed with respect to the reference DO operation. In particular, the higher the EGR rate, the greater the increase in $BSFC_{eq}$. At low EGR levels and with more advanced SOI timings, $BSFC_{eq}$ values are comparable to those of DO combustion. In summary, for the OM2, under low EGR rates and intermediate/advanced diesel SOI, combustion starts earlier and proceeds faster, achieving more favorable in-cylinder conditions, with the combustion phasing closer to the TDCf and higher efficiency, resulting in lower fuel consumption. Conversely, at higher EGR rates and retarded SOI, combustion becomes slower and longer. The $BSFC_{eq}$ of OM1 is 5.4% higher than the DO mode, comparable to the value obtained for OM2 at same EGR rate. Regarding the reduction of CO_2 emissions for the OM2, it remains around 90%, proportional to the HES, varying all the calibration parameters. On the contrary, OM1 exhibits just a moderate decrease in CO_2 emissions (lower than 20%), despite a 30% of HES.

A similar analysis is carried out for pollutant emissions, as reported in Fig. 5, for the same WP. Specifically, from the top, the figure shows the variation in NO_x and Filter Smoke Number (FSN) emissions with

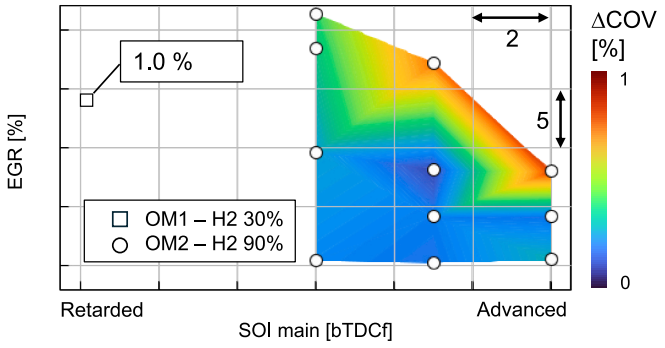

Fig. 3. ΔCOV of the IMEP with respect to the DO mode of different HES and sweep of calibration parameters.

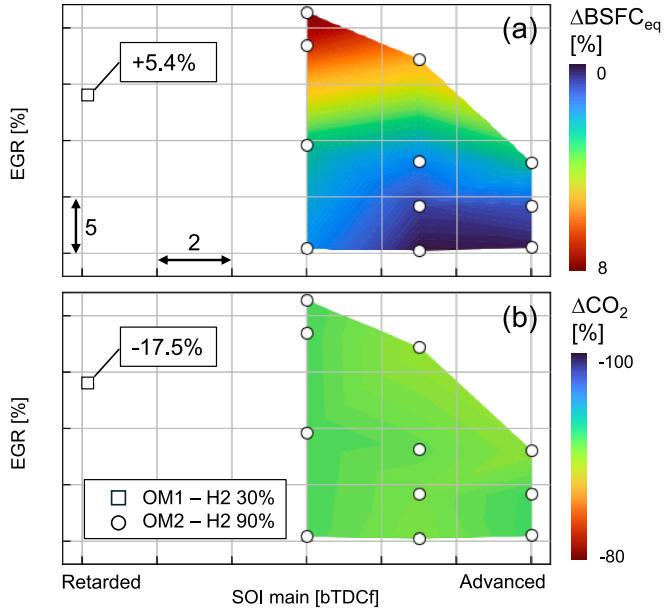

Fig. 4. (a) $\Delta BSFC_{eq}$ and (b) ΔCO_2 with respect to the DO mode of different HES and sweep of calibration parameters.

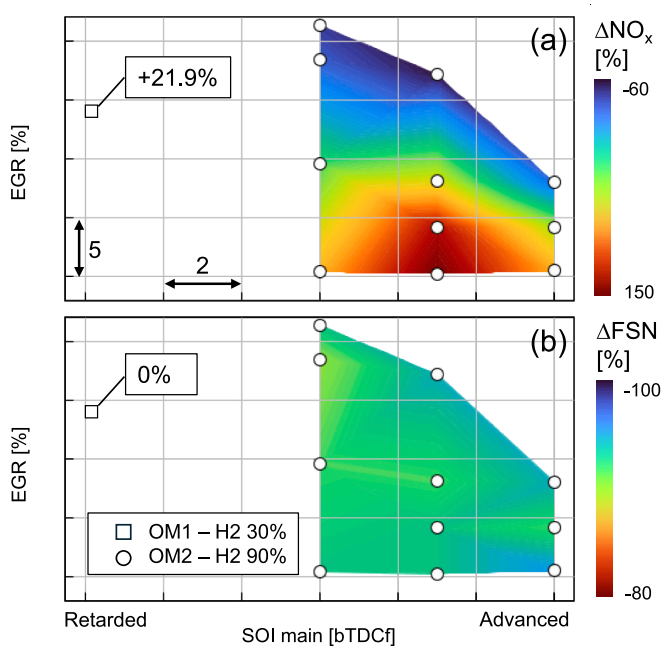

Fig. 5. Impact on pollutant emissions variation with respect to the DO mode of different HES and sweep of calibration parameters. (a) NOx, (b) FSN.

respect to the DO mode.

Regarding NO_x emissions of the OM2, a clear decrease compared to the DO mode is observed at high EGR rates, whereas a significant increase occurs at lower EGR levels. It is worth mentioning that the EGR rate of the DO condition is the higher considered for this WP, and at this level of EGR rate corresponding NOx emissions for the OM2 are lower. In addition, at low EGR rate the highest NO_x emissions are recorded at intermediate SOI timings, confirming observations reported in another DF case study [23] and the relation between the trend in combustion phasing and NOx emissions. In particular, if combustion is triggered near the TDCf higher temperatures are reached at MFB50 with a larger NOx production. This condition is reached for low EGR levels and advanced/intermediate SOI timings. For the OM1, an increase in NOx emissions with respect to the DO mode is present, partially justified by the different levels of EGR rate (i.e., 5% lower EGR rate for OM1). Finally, a substantial reduction in soot emissions is achieved, with decreases of up to 96% relative to the DO reference mode across all operating conditions of OM2. In contrast, OM1 exhibits PM emissions comparable to those of the DO configuration, despite the 30% share of HES. This outcome can be attributed to the lower injection pressure of OM1 compared with the DO mode, which promotes soot formation and is only partially offset by the reduced diesel quantity. Given the complex and highly localized mechanisms governing soot formation and oxidation, a more detailed investigation through high-fidelity 3D-CFD simulations has been required.

3. 3D-CFD simulation setup

The 3D-CFD analysis was carried out by means of a commercially available software, CONVERGE CFD V4.1 [24], in two different steps. Initially, a full-cylinder cold-flow simulation was performed, starting during the exhaust stroke and continuing until the Intake Valve Closing (IVC), in order to model the hydrogen injection and the gas exchange process. In particular, H2 PFI is simulated neglecting injector internal dynamics and imposing an incoming hydrogen mass flow rate on the intake ports, in correspondence of the nozzle of the H2 injector, as highlighted in red in Fig. 6. This first stage of the model aimed to evaluate the in-cylinder thermodynamic conditions, gas exchange, and charge motion up to the end of the compression stroke, accounting for the interaction between the moving geometry, the fluid dynamics, and the hydrogen PFI injection. The full-cylinder simulation was initialized using the 1D-CFD complete engine model results as time-varying boundary conditions. At the IVC, the 3D solution in terms of temperature, pressure, species concentration, and velocity field was mapped across the entire computational domain to provide the initial conditions for the combustion simulation. Differently from previous works focused on diesel engine simulations [25], in the present case, the combustion phase was also simulated under full-cylinder conditions in order to account for potential non-homogeneous hydrogen distribution inside the combustion chamber. The base grid size for all simulations was fixed at 0.5 mm, reaching a minimum cell size of 0.25 mm through specific grid refinement. Owing to this fine base resolution, a fixed first-level embedding was applied near the diesel injector nozzle region to accurately capture spray dynamics. Outside the near-nozzle region, the Adaptive Mesh Refinement (AMR) technique was applied throughout the cylinder volume, thanks to which, the mesh was dynamically refined in regions characterized by high velocity and temperature gradients.

Turbulence was modeled using the RANS-based Re-Normalization Group (RNG) k–ε approach [26]. The spray atomization and droplet breakup were simulated using the Kelvin–Helmholtz and

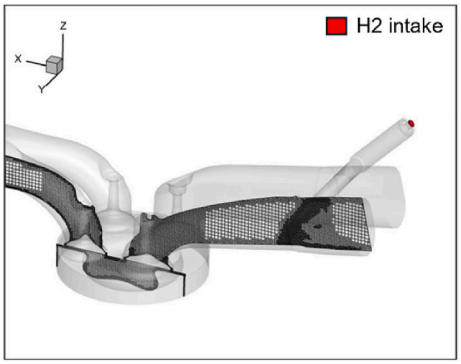

Fig. 6. Mesh refinements during hydrogen injection process, boundary for H2 injection highlighted in red. (For interpretation of the references to colour in this figure legend, the reader is referred to the Web version of this article.)

Rayleigh–Taylor (KH–RT) model [27]. In particular, both models have been calibrated against the available experimental dataset obtained from constant-volume vessel tests. The O'Rourke model was adopted to describe the turbulent dispersion of spray parcels. Droplet collisions were modeled using the No Time Counter (NTC) approach [28], complemented by dynamic droplet drag [29] to account for shape variations. Fuel evaporation was described by the Frossling model [30], converting the evaporated liquid fuel mass into the specified vapor species. The O'Rourke wall-film model was applied for spray–wall interactions. For combustion modeling, the detailed chemistry solver SAGE was employed in combination with the Skeletal Zeuch mechanism, a reduced version of the complete Zeuch mechanism enhanced with soot reaction pathways based on Mauss's work [31]. The mechanism includes 121 species, among which Polycyclic Aromatic Hydrocarbons (PAHs), enabling the use of the particulate mimic model [32], based on the method of moments, to predict the cell-averaged soot mass and number density. Particular attention was devoted to selecting the most appropriate chemical kinetic mechanism for the simulations. Previous studies have clearly shown that hydrogen addition to air strongly influences the autoignition behavior of diesel fuels [33,34]. Depending on the temperature range, hydrogen can either accelerate or inhibit the ignition process, resulting in substantial variations in ignition delay times as a function of the hydrogen mass fraction. To capture this complex behavior, a zero-dimensional (0D) chemical kinetics analysis was conducted by testing several reaction mechanisms. Fig. 7 shows the ignition delay as a function of temperature for different hydrogen mass fractions in a diesel–hydrogen blend, as predicted by the Zeuch mechanism. Two distinct trends can be observed: at higher temperatures, increasing the H_2 mass fraction reduces the ignition delay; at lower temperatures, instead, the presence of hydrogen appears to inhibit ignition. The selected mechanism accurately reproduces the transition region between these two regimes, previously observed in the mentioned literature studies. [33,34], as well as the overall dependence of ignition delay on hydrogen concentration.

All the details of the final simulation setup are listed in Table 3.

4. Results

The abovementioned simulation setup was validated at the WP of Tables 2 and in comparison with the available experimental data. Then, Fig. 8 compares experimental and simulated results for the WP at 2500 rpm and 6 bar BMEP, for different HES. The EGR rate analyzed for OM2 is at medium level. The upper panels display the injection profiles, while the lower panels illustrate the corresponding in-cylinder pressure and Heat Release Rate (HRR) traces. From left to right, the figure presents results for the three operating OMs: DO operation, OM1 with 30% HES, and OM2 with 90% HES. The grey shaded areas indicate the experimental cycle-to-cycle variability considering 100 consecutive cycles. Overall, the simulations show good agreement with the experiments, accurately reproducing the combustion phasing except for a slight

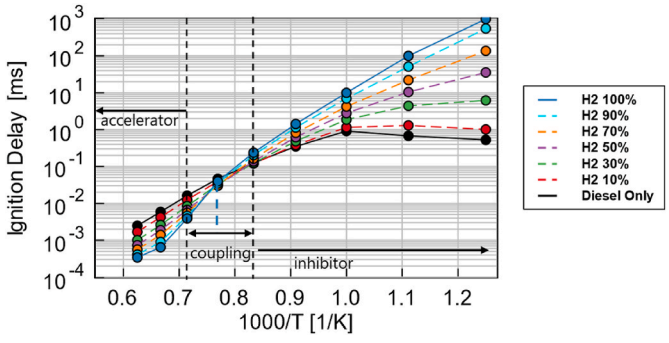

Fig. 7. 0D evaluation of Ignition delay times for diesel/H_2/air flames with different H_2 mass fractions, obtained with the Zeuch mechanism. P = 30 bar.

Table 3
3D-CFD simulation setup.

Minimum grid size	0.25 mm
Turbulence model	RANS – RNG k–ε
Injected fuel (liquid)	Diesel #2
Evaporating species	N-Heptane (N–C7H16)
Spray breakup model	Calibrated KH-RT
Spray/wall interaction model	Wall film model
Combustion model	SAGE detailed chemistry solver
Chemical kinetics	Zeuch mechanism
Soot formation/oxidation model	PM soot model

ignition advance in the DO case. The combustion behavior is well captured in both OM1 and OM2, with simulated pressure traces consistently falling within the experimental variability range. In OM1, the combustion process exhibits multiple stages influenced by the diesel injection pattern, reflecting the interaction between diesel and hydrogen fuels. In contrast, OM2 is characterized by a single, predominantly premixed combustion phase, in which the ignition is triggered by a single diesel pilot injection. To conclude, the developed 3D-CFD model is able to fully characterize either the diesel and the DF combustion behaviour, also in presence of different combustion modes.

Fig. 9 presents a similar comparison for OM2 under varying diesel SOI conditions, for a medium level of EGR rate. Overall, the simulations show good agreement with the experiments, accurately reproducing the combustion phasing, the peak pressure and the HRR curves. The simulated trends varying the diesel SOI are consistent with experimental data, obtaining an anticipated MFB50 and a shorter combustion duration for the case with intermediate SOI. An increase of the experimental COV is evident anticipating the SOI, as already observed in [23]. The COV variation was not captured by the numerical simulations as out of the scope of the analysis. The condition with the intermediate SOI value seems the most promising in terms of combustion efficiency, obtaining an experimental $BSFC_{eq}$ (see Fig. 5) among the closest to the DO reference and was then chosen to be further analyzed in the subsequent 3D-CFD simulations.

Fig. 10 illustrates the outcome of the model for NOx and soot emissions. The top panels show experimental data (black dots) of the Filter Smoke Number (FSN, left axis) compared with simulated soot mass at the Exhaust Valve Opening (EVO) (red dots, right axis). For soot emissions the two considered variables from experiments and simulations are different, but the comparison is consistent in terms of trend. The bottom panels display the corresponding comparison for ISNOx emissions. Results on the left side of the figure are presented as a function of the HES variation (same operating conditions of Fig. 8), while those on the right correspond to variations in diesel SOI (same operating conditions of Fig. 9). The model effectively captures the trends in soot emissions with respect to both calibration parameters, predicting comparable values for DO operation and OM1 with 30% HES, and negligible soot levels for all conditions at 90% HES. Regarding NOx emissions, the model shows good quantitative agreement, with deviations between experimental and simulated values generally within 1 g/kWh, except for the case with retarded SOI. Going from 0 to 90% of HES, the model shows a NOx increase of 40% consistent with 52% of the experiments. On the contrary, anticipating the SOI a 70% of NOx reduction is obtained numerically, consistently with 65% of experiments.

To further characterize the combustion evolution in the different OMs, Fig. 11 presents a 3D analysis for the same operating conditions as in Fig. 8. In the top row, the diesel injection rate (black lines) is shown together with the simulated HRR (red dashed lines). The crank angles corresponding to MFB2, MFB50, and MFB75, used for the 3D snapshots are highlighted. In the subsequent panels, sector views of the combustion chamber focusing on two diesel jets are reported at the selected crank angles, showing an iso-temperature surface representative of the high-temperature flame region (T = 1800 K).

At SOC, ignition occurs between the pilot and main injections in both

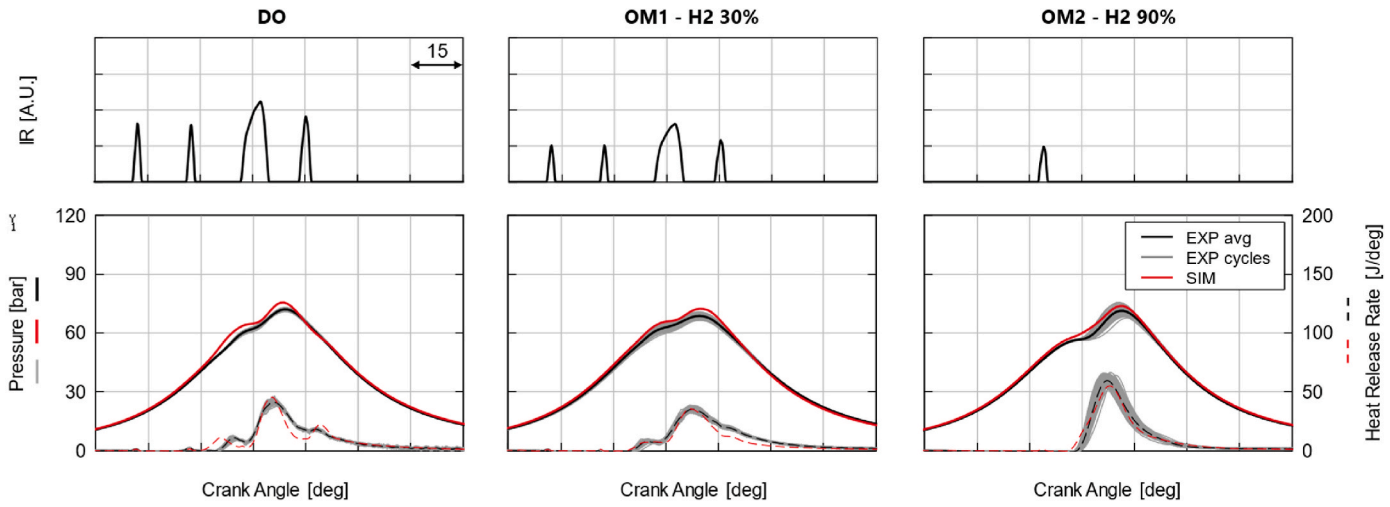

Fig. 8. Simulated (red) vs experimental (black) in-cylinder pressure and heat release rate (bottom), and injection rate (top). Left: DO, center: 30% H2, right: 90% H2. (For interpretation of the references to colour in this figure legend, the reader is referred to the Web version of this article.)

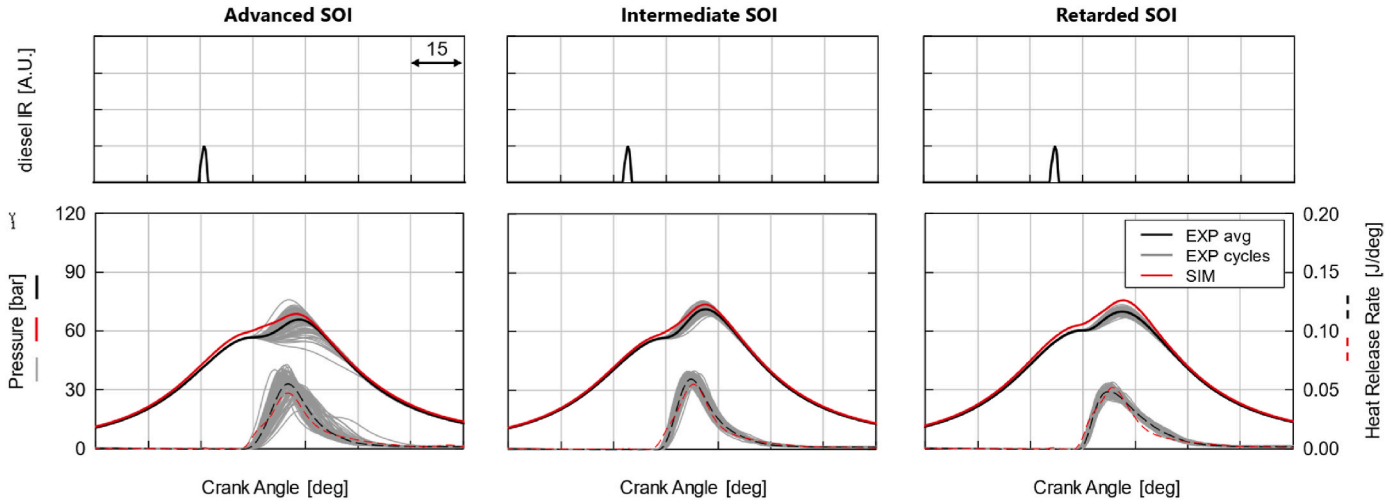

Fig. 9. Simulated (red) vs experimental (black) in-cylinder pressure and burn rate (bottom), and injection rate (top) for the OM2 at 90% of HES and different SOI. Left: advanced SOI, center: intermediate SOI, right: retarded SOI. (For interpretation of the references to colour in this figure legend, the reader is referred to the Web version of this article.)

DO and OM1. Diesel mode exhibits a slightly earlier SOC due to the larger amount of evaporated pilot fuel available for ignition. In addition, hydrogen presence in the mixture could increase the ignition delay of OM1 with respect to DO at this level of temperature. The early flame in diesel mode follows the shape of the fuel plumes, whereas in OM1 the initial kernel appears more localized and nearly spherical. Moreover, due to the lower spray momentum associated with OM1's reduced injection pressure, the in-cylinder swirl motion becomes more evident, as shown by the appearance of a third ignition center near one of the adjacent diesel plumes. The differences in flame topology, elongated in diesel mode and more compact or spherical in OM1, reflect the combined influence of spray momentum and in-cylinder swirl on mixture stratification. In OM2, ignition is significantly delayed with respect to EOI, resulting in predominantly premixed H_2 combustion. The individual ignition kernels in OM2 appear less symmetric than in the other modes.

At MFB50, the diffusive combustion phase develops around the diesel plumes in both diesel and OM1. Diesel mode shows a more intense burn, with a larger fraction of the chamber already involved in the combustion process and visible plume–plume interactions. In OM1, the diesel contribution burns more slowly with a smooth peak of the HRR, due to lower injection pressure and the low turbulence level linked to a typical diesel combustion system that slows down the H2 flame propagation. In OM2, the flame front expands with a distinct morphology, growing almost spherically from the initial kernel toward the walls, following the typical pathway of DF combustion.

By MFB75, most of the mixture in diesel mode is involved in combustion, including the central area and the combustion is shifted to the bottom part of the chamber, following the diesel jet motion that impinges on the walls and comes back guided by the bowl profile. In OM1, the interaction among plumes becomes evident, and a slower jet penetration anchors the combustion in the upper part of the chamber. A slower combustion progression is highlighted by a negligible HRR peak observed during the post-injection event. In OM2, hydrogen combustion is sharper and shorter, in agreement with the more pronounced HRR peak. This is visually confirmed in the iso-temperature fields, where OM2 shows a thinner, more continuous high-temperature shell encompassing most of the chamber. This single-stage, predominantly premixed combustion regime at high HES values aligns with recent observations by Mancaruso et al. [35], where hydrogen enrichment was found to shorten the combustion duration.

To conclude, a characterization of the in-cylinder conditions leading

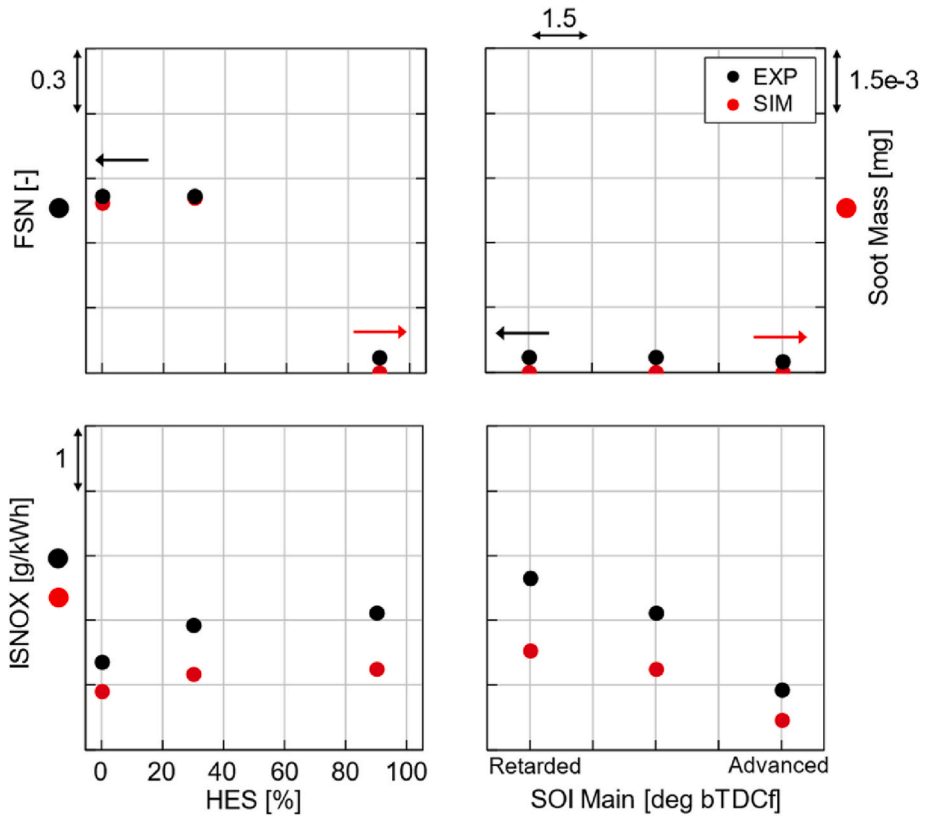

Fig. 10. Simulated (red) vs experimental (black) soot emissions (top) and ISNOx (bottom), as a function of HES (left) and SOI (right). (For interpretation of the references to colour in this figure legend, the reader is referred to the Web version of this article.)

to soot formation and oxidation processes is carried out for the same HES variation as in Fig. 11. In particular, contour plots of the temperature and O_2 mass fraction are reported in Fig. 12 on two slices aligned with two spray jets, together with a selected isosurface of soot volume to highlight regions of high soot concentration, at three different crank angles. In the top row of the figures, the diesel injection rate is recalled together with the evolution of the total soot mass in the cylinder. The crank angles used for the 3D snapshots are also highlighted with black dashes on the top.

- At θ_1: For the DO and OM1 modes, the main injection event is concluded, and soot production starts to rise. Owing to the higher momentum of the liquid jet in DO mode, combustion is shifted along the spray axis and into the lower part of the combustion chamber. Here favorable temperature distribution and oxygen deficiency promote larger soot formation compared to OM1. The soot-rich zones coincide with regions of elevated temperature and low O_2 availability towards the tip of the jet, as seen in the corresponding O_2 contours. Conversely, in OM1, the liquid plume remains away from the walls and combustion evolves near the center of the cylinder, where soot starts to form. The more confined and lifted flame in OM1 produces smaller, centrally located soot rich regions compared with the extended soot cloud in diesel mode. No soot production is observed in OM2, thanks to both the lower temperatures reached and the higher O_2 distribution associated with the higher HES fraction.
- At θ_2: For the DO and OM1 modes, the post-injection event is nearly concluded. The jet penetration in DO mode is higher (visible as a blue region in the temperature map), reaching an area where a high level of oxygen is available around the diesel plume, thanks to the fact that the diesel main injection burns in the lower part of combustion chamber. In OM1, the slower liquid penetration keeps the ignition along the jet plume near the chamber center where oxygen deficiency continues to promote soot formation. In OM2, the flame propagates spherically, impinging on the chamber walls and expanding toward the center in a predominantly premixed mode, with no soot formation.
- At θ_3: In DO mode, the combustion moves toward the bowl center thanks to the jet momentum, where a wide high-temperature region driven by the post combustion and the available oxygen presence favors soot oxidation. The O_2 distribution also indicates localized re-entrainment of fresh oxygen near the bowl center, reinforcing oxidation processes. This is highlighted also by the soot mass curve on the top, showing a clear decrease, and by the visible reduction of the soot volume in the 3D field, confirming the effectiveness of the jet momentum in the post injection strategy to enhance soot oxidation [36]. In contrast, in OM1, the combustion process remains confined to the lower part of the chamber, where low temperature and oxygen scarcity hinder soot oxidation, as indicated by the flat soot mass curve and the persistent low-O_2 zones. Hence, in OM1, the post-injection strategy is not effective in promoting soot oxidation. In OM2, combustion involves available H2 in the chamber with no soot formation.

Overall, the evolution of the in-cylinder conditions clearly confirms an excellent soot-oxidation capability driven by the post injection event in the DO mode. On the contrary, in OM1 the post-injection event is not effective in promoting soot oxidation: the lower spray momentum and the limited oxygen availability in the lower bowl region inhibit the re-entrainment of fresh air, resulting in persistent high-soot zones. This finding aligns with the observations of Tripathi et al. [17], who reported that, in DF hydrogen–diesel engines with split injection, soot oxidation is hindered by oxygen-depleted regions at the center of the bowl, where low-temperature conditions prevent effective burnout of soot. Similarly, Vávra et al. [15] noted that, at higher HES the displacement of intake oxygen by hydrogen becomes the dominant factor controlling PM formation and oxidation process, limiting oxidation efficiency even when

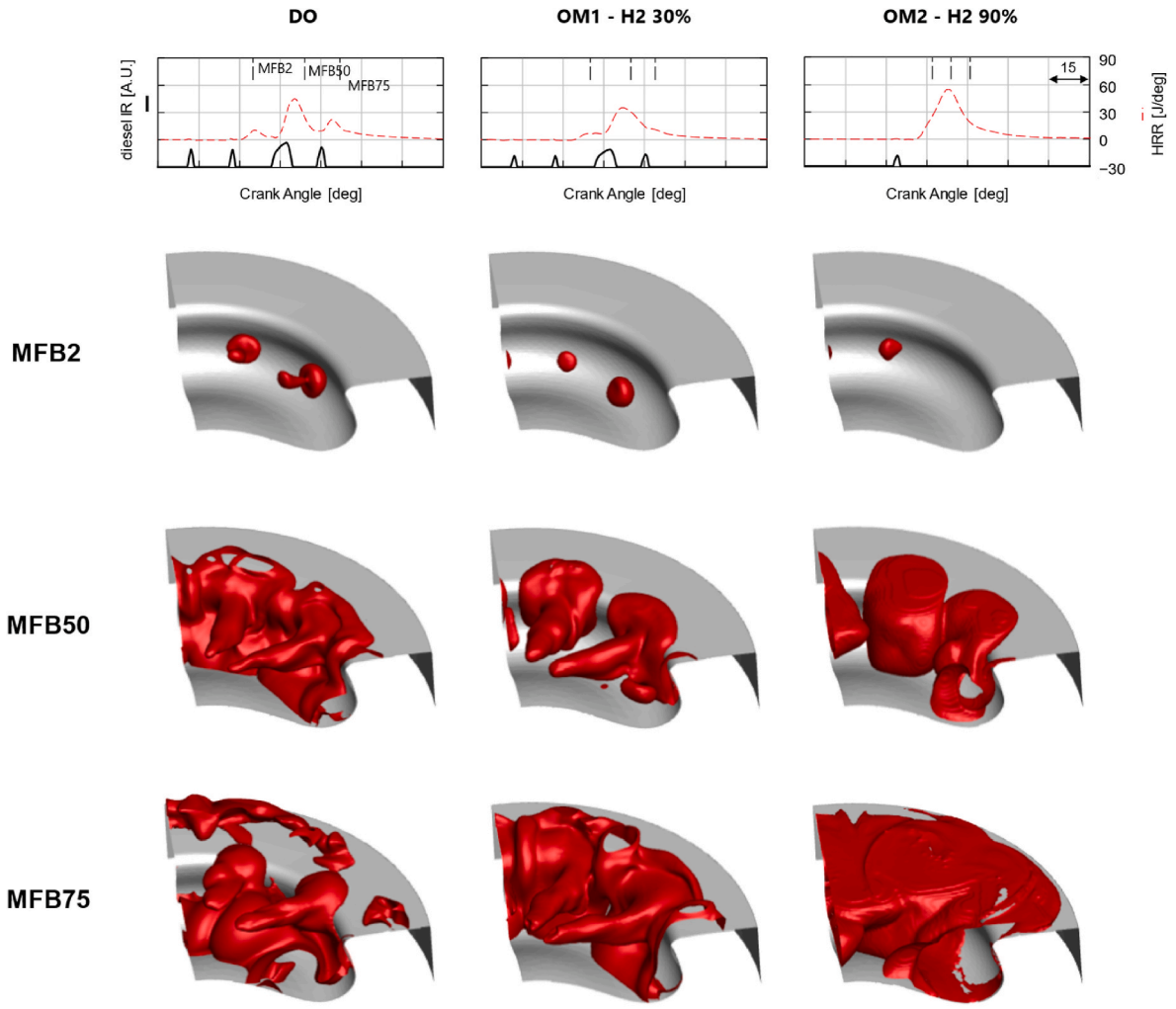

Fig. 11. Top: Diesel IR and simulated HRR. Bottom: Isosurface of temperature (T = 1800K) for the chosen HES at MFB2, MFB50 and MFB75.

overall soot formation decreases. These consistent results suggest that, under DF operation, the lack of oxygen in localized regions and the altered mixing dynamics introduced by hydrogen addition both constrain the post-injection soot oxidation mechanisms that are otherwise effective in conventional diesel combustion. Finally, OM2, confirms the fully premixed nature of H_2 combustion and the subsequent absence of soot formation thanks to the limited amount of diesel involved in the combustion.

Although the developed CFD framework demonstrated good agreement with the experimental measurements and proved effective in capturing the main combustion and emission trends, some limitations of the present study should be highlighted. First, the presented analysis focuses on a single representative engine operating point (2500 rpm, 6 bar BMEP). The generalization of the results to other operating conditions, loads, and engine speeds has been preliminarily investigated, but these results are not presented in this study and will be addressed in future work. Second, the SAGE combustion model, based on the well-stirred reactor approach, may limit the capability to fully capture turbulence–chemistry interactions. Finally, the use of a RANS turbulence model focuses only on the average engine behavior and is therefore unable to reproduce the well-known cycle-by-cycle variability observed experimentally.

5. Conclusions

This work presented a comprehensive CFD-supported methodology for the analysis and optimization of hydrogen–diesel Dual-Fuel (DF) combustion systems, calibrating a detailed 3D simulations on an extensive experimental database. The developed framework was applied to two distinct Operating Modes (OMs) of a medium-duty compression ignition engine: a retrofit DF configuration (OM1), in which the original diesel multi-pulse injection strategy was preserved, and a native DF calibration (OM2) specifically optimized for high Hydrogen Energy Share (HES) operation with a single pilot diesel injection.

The results demonstrated that these two operating modes exhibit fundamentally different combustion behaviors. In the retrofit configuration (OM1), hydrogen presence in the in-cylinder mixture contributes to a longer ignition process, and the retained diesel multi-pulse injection produces a mixed diffusive–premixed combustion regime. Conversely, in the native DF configuration (OM2), the single pilot event promotes predominantly premixed combustion. This configuration results in shorter combustion duration, and more homogeneous temperature distribution. The transition from OM1 to OM2 thus represents a shift from diffusion-controlled to fully premixed combustion typical DF combustion, confirming the strong coupling between diesel injection characteristics and HES.

The distinct combustion regimes are reflected in the emission behavior. In OM1, limited air entrainment and the persistence of oxygen-depleted regions near the lower bowl promote soot formation during the main and post-injection phases, while the reduced spray momentum prevents effective air entrainment in the combustion region and subsequently the soot oxidation. Consequently, particulate

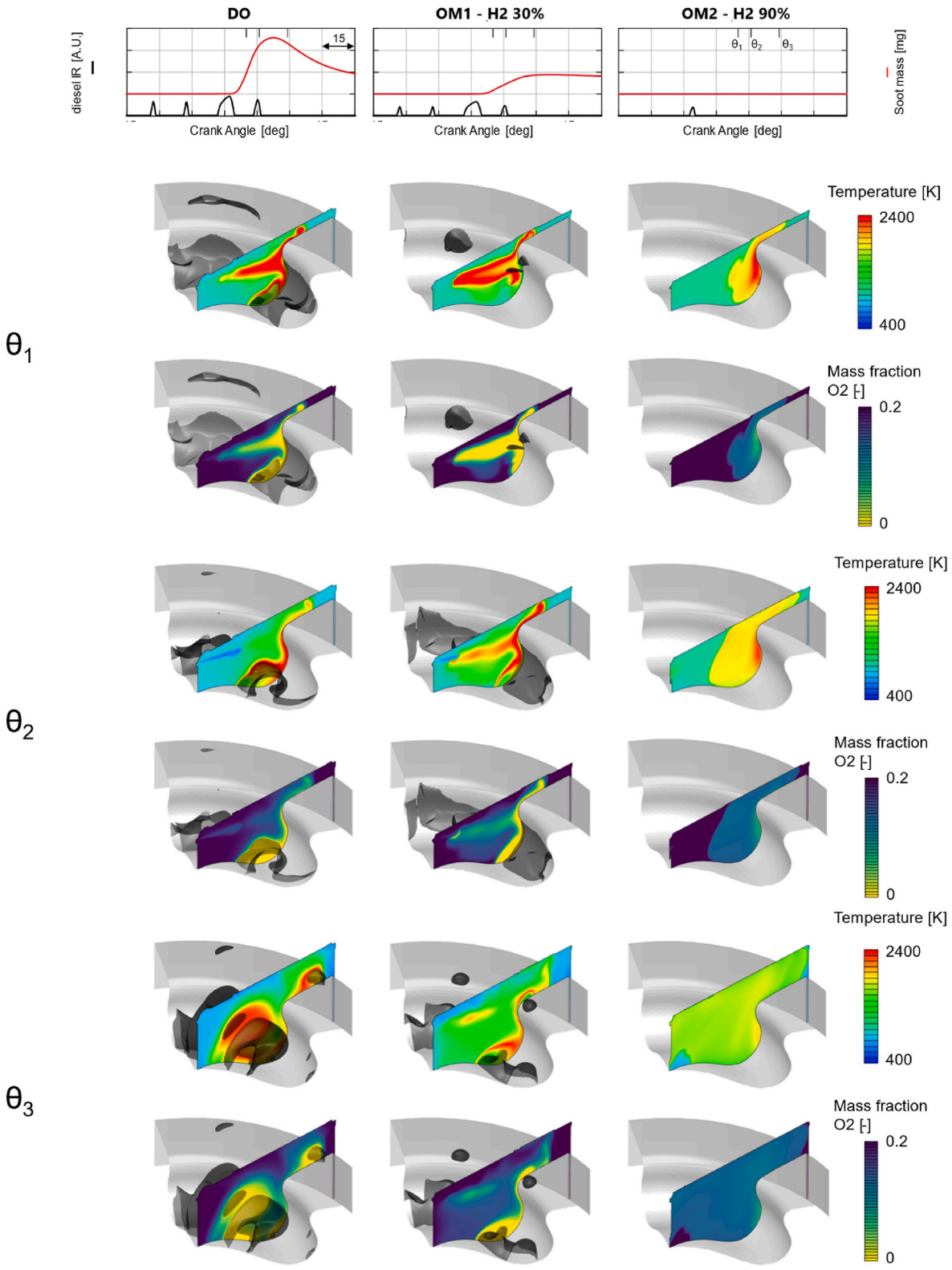

Fig. 12. Contour plots of the temperature and O2 mass fraction distribution for the chosen HES at three different crank angles. Isosurface of high soot volume concentration in black.

emissions remain comparable to diesel operation despite 30% of HES. In contrast, OM2 achieves nearly complete soot elimination, with reductions of up to 96%, due to hydrogen's carbon-free nature and the homogeneous in-cylinder conditions that prevent soot formation. These findings confirm that the increase of HES alone does not guarantee optimal DF performance, as pollutant formation mechanisms remain strongly influenced by the diesel injection strategies and local thermodynamic conditions.

Overall, the study highlights the decisive role of the diesel calibration strategy, its timing, pressure, and mass, influencing ignition

dynamics, combustion efficiency, and pollutant formation. A proper dual-fuel calibration must therefore combine an optimized HES with a dedicated diesel injection strategy to ensure stable combustion and enhanced soot emissions abatement. The developed and validated 3D-CFD framework proved effective in capturing the coupled effects of injection dynamics, hydrogen–air mixing, and detailed chemical kinetics, providing a predictive tool for the design of next-generation hydrogen–diesel DF engines.

CRediT authorship contribution statement

B. Peiretti Paradisi: Writing – original draft, Visualization, Validation, Methodology, Investigation, Formal analysis, Data curation. **A. Piano:** Writing – review & editing, Visualization, Supervision, Methodology, Investigation, Conceptualization. **F. Millo:** Project administration, Funding acquisition. **F. Accurso:** Writing – review & editing, Project administration, Methodology, Data curation, Conceptualization. **F.C. Pesce:** Supervision, Project administration, Conceptualization. **A. Vassallo:** Supervision, Project administration, Funding acquisition.

Declaration of competing interest

The authors declare that they have no known competing financial interests or personal relationships that could have appeared to influence the work reported in this paper.

Acknowledgments

The research presented was performed within the project: “Piattaforma motore a combustione interna alimentato a idrogeno (H2 ICE)” funded by “Ministero delle Imprese e del Made in Italy” inside call “Accordi per l'innovazione” and approved by “Decreto n. 2098 del July 06, 2023”.

Abbreviations

3D-CFD	Three-Dimensional Computational Fluid Dynamics
AMR	Adaptive Mesh Refinement
BMEP	Brake Mean Effective Pressure
$BSFC_{eq}$	Equivalent Brake Specific Fuel Consumption
CI	Compression Ignition
DF	Dual Fuel
DO	Diesel Only
ECU	Engine Control Unit
EGR	Exhaust Gas Recirculation
EOI	End of Injection
EVO	Exhaust Valve Opening
FSN	Filter Smoke Number
HES	Hydrogen Energy Share
HRR	Heat Release Rate
ICE	Internal Combustion Engine
IVC	Intake Valve Closing
LHV	Lower Heating Value
MFB	Mass Fraction Burned
NO_x	Nitrogen Oxides
OM	Operating Mode
PFI	Port Fuel Injection
PM	Particulate Matter
SOC	Start of Combustion
SOI	Start of Injection
WP	Working Point

References

[1] Dornoff J, Rodríguez F. Euro 7: the new emission standard for light- and heavy-duty vehicles in the European Union, ICCT policy update. https://theicct.org/wp-content/uploads/2024/03/ID-116-–-Euro-7-standard_final.pdf; 2024.
[2] Smith D, Graves R, Ozpineci B, Jones PT, Lustbader J, Kelly K, Walkowicz K, Birky A, Payne G, Sigler C, Mosbacher J. Medium-and heavy-duty vehicle electrification an assessment of technology and knowledge gaps. https://info.ornl.gov/sites/publications/Files/Pub136575.pdf; 2019.
[3] Fleming, K.L., Brown, A.L., Fulton, L., and Miller, M., “Electrification of Medium- and heavy-duty ground transportation: status report,” doi:10.1007/s40518-021-00187-3/Published.
[4] European Parliament. Fit for 55: delivering the EU's 2030 climate target on the way to climate neutrality. https://eur-lex.europa.eu/legal-content/EN/TXT/?uri=CELEX%3A52021DC0550; 2021.
[5] Martins J, Brito FP. Alternative fuels for internal combustion engines. Energies 2020;13(15). https://doi.org/10.3390/en13164086.
[6] Onorati A, Payri R, Vaglieco BM, Agarwal AK, Bae C, Bruneaux G, Canakci M, Gavaises M, Günthner M, Hasse C, Kokjohn S, Kong SC, Moriyoshi Y, Novella R, Pesyridis A, Reitz R, Ryan T, Wagner R, Zhao H. The role of hydrogen for future internal combustion engines. Int J Engine Res 2022;23(4):529–40. https://doi.org/10.1177/14680874221081947.
[7] Oktar HE, Tonyali IH, Apaydin AH. A cost-effective and sustainable path to a green future: retrofitting internal combustion engines for hydrogen fuel utilization. Int J Hydrogen Energy 2025;143:969–77. https://doi.org/10.1016/j.ijhydene.2024.12.240.
[8] Peiretti Paradisi B, Pulvirenti L, Vinogradov A, Rolando L, Piano A, Millo F, Prussi M. A techno-economic life cycle assessment of H2 fuelled and electrified urban buses. Appl Energy 2025;401. https://doi.org/10.1016/j.apenergy.2025.126738.
[9] Yip HL, Srna A, Yuen ACY, Kook S, Taylor RA, Yeoh GH, Medwell PR, Chan QN. A review of hydrogen direct injection for internal combustion engines: towards carbon-free combustion. Applied Sciences (Switzerland) 2019;9(22). https://doi.org/10.3390/app9224842.
[10] Du H, Chai WS, Wei H, Zhou L. Status and challenges for realizing low emission with hydrogen ultra-lean combustion. Int J Hydrogen Energy 2024;57:1419–36. https://doi.org/10.1016/j.ijhydene.2024.01.108.
[11] Dimitriou P, Tsujimura T. A review of hydrogen as a compression ignition engine fuel. Int J Hydrogen Energy 2017;42(38):24470–86. https://doi.org/10.1016/j.ijhydene.2017.07.232.
[12] Hosseini SH, Tsolakis A, Alagumalai A, Mahian O, Lam SS, Pan J, Peng W, Tabatabaei M, Aghbashlo M. Use of hydrogen in dual-fuel diesel engines. Prog Energy Combust Sci 2023;98. https://doi.org/10.1016/j.pecs.2023.101100.
[13] Stewart J, Clarke A. A three-zone heat-release rate model for dual-fuel combustion. Proc Inst Mech Eng C J Mech Eng Sci 2010;224(11):2423–34. https://doi.org/10.1243/09544062JMES1955.
[14] Xin Q, Pinzon CF. Improving the environmental performance of heavy-duty vehicles and engines: key issues and system design approaches. In: Alternative fuels and advanced vehicle technologies for improved environmental performance:

towards zero carbon transportation. Elsevier Inc.; 2014. p. 279–369. https://doi.org/10.1533/9780857097422.2.279. ISBN 9780857095220.
[15] Vavra J, Bortel I, Takats M. A dual fuel hydrogen - diesel compression ignition engine and its potential application in road transport. In: SAE technical papers 2019-01-0564; 2019. https://doi.org/10.4271/2019-01-0564.
[16] Tsujimura T, Suzuki Y. The utilization of hydrogen in hydrogen/diesel dual fuel engine. Int J Hydrogen Energy 2017;42(19):14019–29. https://doi.org/10.1016/j.ijhydene.2017.01.152.
[17] Tripathi G, Sharma P, Dhar A, Sadiki A. Computational investigation of diesel injection strategies in hydrogen-diesel dual fuel engine. Sustain Energy Technol Assessments 2019;36. https://doi.org/10.1016/j.seta.2019.100543.
[18] Scrignoli F, Pisapia AM, Savioli T, Mancaruso E, Mattarelli E, Rinaldini CA. Exploring hydrogen–diesel dual fuel combustion in a light-duty engine: a numerical investigation. Energies 2024;17(22). https://doi.org/10.3390/en17225761.
[19] Maroteaux F, Sebai S, Mancaruso E, Rossetti S, Schembri P, Radja K, Barichella A. Numerical and experimental analysis of dual fuel hydrogen/diesel combustion at varying engine speed on a single cylinder engine. In: SAE technical papers 2024-24-0044; 2024. https://doi.org/10.4271/2024-24-0044.
[20] Guan M, Rochussen J, Steiche P, Sapkota N, Farzam R, McTaggart-Cowan G, Rogak SN, Kirchen P. Characterizing hydrogen-diesel dual-fuel performance and emissions in a commercial heavy-duty diesel truck. Int J Hydrogen Energy 2024;86:1085–96. https://doi.org/10.1016/j.ijhydene.2024.08.480.
[21] Lee T, Rajasegar R, Srna A. Understanding the interplay between pilot fuel mixing and auto-ignition chemistry in hydrogen-enriched environment. Proc Combust Inst 2024;40(1–4). https://doi.org/10.1016/j.proci.2024.105351.
[22] Golisano R, Scalabrini S, Arpaia A, Pesce F, Vassallo A, Borgia F, Cubito C, Biasin V, Knichel T, Millo F, Rolando L, Piano A. Hydrogen internal combustion engine & KERS: an appealing value-proposition for green power pack. In: 42nd international Vienna motor symposium; 2021.
[23] García Valladolid P, Tunestål P, Monsalve-Serrano J, García A, Hyvönen J. Impact of diesel pilot distribution on the ignition process of a dual fuel medium speed marine engine. Energy Convers Manag 2017;149:192–205. https://doi.org/10.1016/j.enconman.2017.07.023.
[24] Richards KJ, Senecal PK, Pomraning E. Converge 4. 2024.
[25] Millo F, Piano A, PeirettiParadisi B, Marzano MR, Bianco A, Pesce FC. Development and assessment of an integrated 1D-3D CFD codes coupling methodology for diesel engine combustion simulation and optimization. Energies 2020;13(7). https://doi.org/10.3390/en13071612.
[26] Orszag SA, Yakhot V, Flannery WS, Boysan F, Choudhury D, Maruzewski J, Patel B. Renormalization Group modeling and turbulence simulations. Near-Wall Turbulent Flows; 1993. p. 1031–46.
[27] Reitz RDBF. Mechanisms of breakup of round liquid jets. Encyclopedia Fluid Mech 1986;3:233–49.
[28] Schmidt DP, Rutland CJ. A new droplet collision algorithm. J Comput Phys 2000;164(1):62–80. https://doi.org/10.1006/jcph.2000.6568.
[29] O'Rourke PJ, Amsden AA. The TAB method for numerical calculation of spray droplet breakup. NM (USA): Los Alamos National Lab 1987.
[30] Amsden A, O'Rourke P, Butler T. KIVA-II: a computer program for chemically reactive flows with sprays, Technical Report LA-11560-MS, UC-96. Los Alamos National Lab. (LANL); 1989.
[31] Zeuch T, Moréac G, Ahmed SS, Mauss F. A comprehensive skeletal mechanism for the oxidation of n-heptane generated by chemistry-guided reduction. Combust Flame 2008;155(4):651–74. https://doi.org/10.1016/j.combustflame.2008.05.007.
[32] Kazakov A, Frenklach M. Dynamic modeling of soot particle coagulation and aggregation: implementation with the method of moments and application to high-pressure laminar premixed flames. Combust Flame 1998;114(3–4):484–501. https://doi.org/10.1016/S0010-2180(97)00322-2.
[33] Gong X, Wang X, Zhou H, Ren Z. Laminar flame speed and autoignition characteristics of surrogate jet fuel blended with hydrogen. Proc Combust Inst 2023;39(2):1773–81. https://doi.org/10.1016/j.proci.2022.07.162.
[34] An H, Yang WM, Maghbouli A, Li J, Chou SK, Chua KJ. A numerical study on a hydrogen assisted diesel engine. Int J Hydrogen Energy 2013;38(6):2919–28. https://doi.org/10.1016/j.ijhydene.2012.12.062.
[35] Mancaruso E, Robbio R De, Vaglieco BM. Hydrogen/diesel combustion analysis in a single cylinder research engine. In: SAE technical papers 2022-24-0012; 2022. https://doi.org/10.4271/2022-24-0012.
[36] Millo F, Piano A, Peiretti Paradisi B, Boccardo G, Mirzaeian M, Arnone L, Manelli S. The effect of post injection coupled with extremely high injection pressure on combustion process and emission formation in an off-road diesel engine: a numerical and experimental investigation. In: SAE Technical Paper 2019-24-0092 1; 2019. https://doi.org/10.4271/2019-24-0092.